

## Cite this article

Nadi A, Saleh A and Ayazi A

Low-cycle fatigue analysis of a new type of reduced-beam-section connection. *Proceedings of the Institution of Civil Engineers – Structures and Buildings*, <https://doi.org/10.1680/jstbu.20.00199>

## Research Article

Paper 2000199

Received 11/08/2020;  
Accepted 21/10/2020

ICE Publishing: All rights reserved

# Low-cycle fatigue analysis of a new type of reduced-beam-section connection

Amir Nadi PhD

Department of Civil Engineering, Khorramabad Branch, Islamic Azad University, Khorramabad, Iran

Aboozar Saleh PhD

Department of Civil Engineering, Professor Hesabi Branch, Islamic Azad University, Tafresh, Iran

Amir Ayazi PhD

Department of Civil Engineering, Shahr-e-Qods Branch, Islamic Azad University, Tehran, Iran (Orcid:0000-0002-1914-4659)

(corresponding author: a.ayazi@qodsiau.ac.ir)

**Stress concentrations in a new type of reduced-beam-section (RBS) connection were investigated. Experimental and numerical results of RBS connections with semilunar web (SW) and holed tubular webs (HTW) were compared with connections with tubular webs (TW). For the SW, two semi-circular plates were used in place of a flat web in the beam. For the HTW, a steel tube was used instead of part of the beam web and holes were created in the beam web. For the TW, a steel tube was used instead of part of the beam web but without holes. The connections had adequate shear capacity but made little contribution to flexural stiffness and capacity. Semi-deep beam specimens were fabricated and tested under cyclic loading. The results showed that the beam connections with SWs and HTWs had 30% and 20% less fatigue damage respectively than those with TWs. The storey drift capacity was also increased to 7%, much more than that stipulated by current seismic codes. The specimens were modelled using finite-element software to validate the experimental results.**

## Notation

$B$	distance of the center of the semilunar parts from the edge of the beam
$b$	fatigue strength exponent
$b_f$	width of the beam
$c$	fatigue ductility exponent
$D$	cumulative fatigue damage
$D_s$	diameter
$E$	elastic modulus
$K$	constant
$k$	number of blocks
$m$	slope of fatigue curve
$N_f$	number of cycles to failure
$N_{f_i}$	number of cycles to failure at rotation range $\Delta\phi_i$
$n_i$	number of cycles to reach rotation range $\Delta\phi_i$
$S$	perpendicular length between two edges of semi-circular parts
$t$	thickness of the beam
$\Delta\varepsilon$	strain range
$\Delta\phi$	total rotation range
$\varepsilon$	strain
$\varepsilon_y$	yield of strain
$e'_f$	fatigue ductility coefficient
$\sigma'_f$	fatigue strength coefficient

reasons for brittle fracture is low-cycle fatigue (LCF) in connections under seismic loading (Huang and Mahin, 2010; Lashkari, 1988; Nastar *et al.*, 2012; Tateishi and Hanji, 2004). LCF is caused by repeated inelastic strains in the material at a small number of load cycles.

In the current seismic design codes, fatigue is not considered in the design of moment frame systems subjected to seismic loadings (AISC, 2010; BSI, 2004). Ricles *et al.* (2000) studied LCF in ductile welded unreinforced flange connections and presented a method to find cracks under low-cycle loadings. Ricles *et al.* (2002) showed that cracks occurred in beam flange welds due to heat of welding and weld access holes. Barsom (2000) studied one of the important parameters (LCF damage) in connection failures. The assessment of LCF damage to connections in seismic moment frame systems is necessary for the design and behaviour predictions of connections under seismic loading. Fatigue life in a connection under low-cycle loading with a large plastic strain range is calculated by the Manson–Coffin rule (Coffin, 1954; Manson, 1954). For the assessment of cumulative fatigue damage, the Palmgren–Miner rule is used (Miner, 1945; Palmgren *et al.*, 1924). Zhou *et al.* (2014) studied the behaviour of steel moment resisting frames under cyclic tests. To assess the welded connections, seven connections were tested under low-cycle loading. They then presented a method for the assessment of LCF in welded connections under seismic loading using the Palmgren–Miner rule (Zhou *et al.*, 2014). Amiri and Anderson (2012) studied LCF in steel moment-resisting frames. They presented an analysis of LCF in reduced-beam-section (RBS) connections in a nine-floor building and calculated the damage in the connections. The stress concentration in RBS connections is an important factors in failure of the connection. In RBS

## 1. Introduction

After the 1994 Northridge earthquake, many studies on the ductile behaviour of welded or bolted connections were conducted (Kuwamura, 1998). In many beam–column connections in moment frame systems, brittle fractures occur (Malley, 1998; Ricles *et al.*, 2000), and a lot of damage to connections is due to low-cycle loads (Nastar *et al.*, 2010). One of the

connections, the flange width is reduced. This reduction first causes local buckling and then lateral torsion in the connection.

Many experimental and numerical assessments of the seismic behaviour of RBS connections for steel building structures have been conducted (Uang and Chi, 2002; Zhang and Ricles, 2006). The studies show that, due to the reduced flange width, local buckling in the beam web decreases (Jones *et al.*, 2002). Usually, failure as a result of LCF in the reduced region occurs after local buckling of the beam flanges due to large plastic range in the plastic hinge (Lee, and Stojadinovic, 2004). LCF and fatigue damage have been investigated in several studies (Bhatti *et al.*, 2019; Deng *et al.*, 2018, 2020; Kosec *et al.*, 2019; Papagianni and Wahab, 2020; Pereira and Wahab, 2020; Wang *et al.*, 2018, 2019; Zhang *et al.*, 2018).

Mirghaderi *et al.* (2010) proposed an accordion web (AW) beam, replacing two angles symmetrically, instead of a flat web. The idea was to move the plastic hinge to a desirable place and far from the column face. In that study, fracture in the angle occurred due to the stress concentration. An AW with the flat web replaced by a tube was introduced by Zahrai *et al.* (2017a): a tube was placed symmetrically at a certain distance from the edge of the column in order to create a plastic hinge there, and there was no damage to the column. Due to the lower width to thickness ratio at the location of the tube, lateral torsional buckling did not occur. Saleh *et al.* (2016a) also suggested using a tube as an AW in deep beams. In this method, due to the removal of sharp corners of the angles and the use of a tubular web (TW), better behaviour of the connection under LCF was observed. The results showed that the use of a TW-RBS, like the AW-RBS, reduced the plastic moment of the section in the area where the tube is placed, the plastic hinge is guided to that area and there was no damage in other areas. According to the results, the TW-RBS satisfied the ANSI/AISC 341-10 specifications for rigid connections (AISC, 2010) and the recommendations of Fema-355D (Fema, 2000) and also increased the floor drift by 6%. Zahrai *et al.* (2017a, 2017b) suggested the idea of increasing the length of plastic hinges by placing two tubes together. In this case, the demand of the beam-column connection in identical storey drifts was reduced by more than 30%. That connection also complied with the specifications for rigid connections (AISC, 2010; Fema, 2000) and increased storey drift by 6%. The results of the study were very satisfactory in comparison with numerical analyses. Imanpour *et al.* (2019) used two angles instead of a flat web. A seismic design method was developed for this double-angle AW-RBS connection in the framework of US steel design standards. The plastic hinge was transferred to the desired point. Imanpour *et al.* (2019) provided a comparison of experimental and numerical results, and showed that the connection satisfied the AISC (2010) and Fema (2000) requirements regarding flexural rigid connections without any instability or resistance loss. A reliable and stable plastic hinge rotation was achieved without significant local and global instability under cyclic loading.

In the work reported in this paper, two AW-RBSs of semi-deep beams under stress concentration due to LCF were compared. One RBS was made by using two circular arcs on both sides of the web instead of a flat web (semilunar web (SW)). In the other, holes were created in the web (holed tubular web (HTW)) of the beam at the connection of the tube to the web (HTW-RBS), as first proposed by Nadi *et al.* (2020). It was anticipated that the proposed SW-RBS and HTW-RBS connections could reduce the damage caused by LCF by about 30% as compared with TW-RBS connections. Reducing fatigue damage in the connections would prevent separation of the beam flange from the beam web at the plastic hinge. In turn, this increases the ductility of the joint, prevents buckling and increases the flexural capacity of the connection. It also prevents brittle plastic hinge failure. In addition to improving the energy dissipation, the SW-RBS and HTW-RBS connections can reduce the demand of beam-column connections by about 30% compared with TW-RBS connections. In both of the proposed connections, due to reduced fatigue damage, local and global buckling is prevented under cyclic loading. The experimental results obtained in this work were compared with the numerical modelling results obtained from finite-element (FE) analyses.

## 2. Proposed connections

The configurations of the SW-RBS and HTW-RBS connections are shown in Figure 1. As shown in Figure 1(a) a steel tube is placed on the web of the beam and near the column instead of flat web. Holes are created on the web of beam at the connection of tube to web (Nadi *et al.*, 2020). As shown in Figure 1(b), two arcs are placed instead of the web. A view of the flange at the location of semi-circular parts is also shown in Figure 1(b). Due to the arcs and the tube in the SW-RBS and HTW-RBS connections, respectively, the out-of-plane stiffness of the AW is increased. Based on this accordion-like behaviour of the corrugated web, the contribution of the beam web to the beam bending moment is expected to be negligible within the corrugated region.

The existence of an arc region in the two connections provides a better condition than a corrugated web connection under LCF, by changing the sharp corners of angles to an arc shape. The stability and ductility of the beam with the TW-RBS (Saleh *et al.*, 2016b) connection is then improved within the plastic hinge region. The connections were used in semi-deep beams. The semi-deep beams are affected by the geometry, loading and the span to height ratio, which defines the boundary between bending and shearing behaviour of the beam. That is, if the height of the beam is increased it performs bending and if the height of the beam is decreased it performs shearing. For heights between these two states, which has same function boundary as shearing and bending, beams are called semi-deep.

## 3. Test programme

Experiments were conducted to compare the effect of increasing the length of the plastic hinge of the SW-RBS flexural

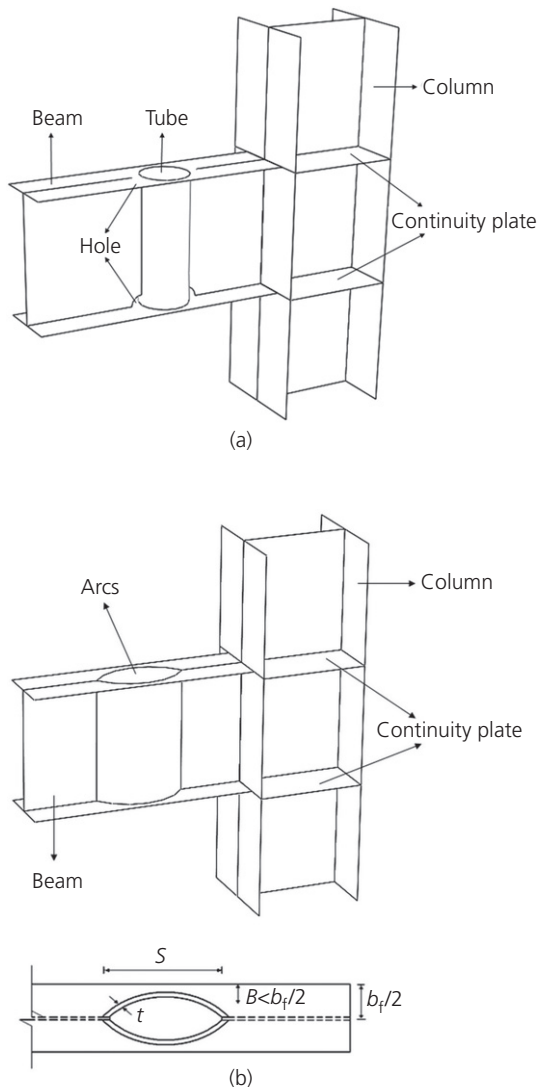


**Figure 1.** Overall view of specimens: (a) proposed HTW-RBS connection; (b) proposed SW-RBS connection and view of the flange at the location of the semi-circular parts

connection under LCF. The results obtained were compared with the results reported by Nadi *et al.* (2020).

### 3.1 Test specimens

SW-RBS and HTW-RBS connections were fabricated for testing. The test specimens were external beam to column connections. The beams and columns were selected to be half of a full-scale model. In the experimental tests, the beam was horizontal and the column was vertical. The weak beam–strong column criterion was used to ensure the formation of a plastic mechanism in the beam. An H-shaped column with a  $30 \times 260 \text{ cm}^2$  plate for the web and two  $20 \times 260 \text{ cm}^2$  plates for the flanges was used. The beam was also made of  $10 \times 300 \text{ cm}^2$  plates for the web and two  $12 \times 150 \text{ cm}^2$  plates for the flanges. A web plate of 15 mm thickness was used from

the beginning of the web to the column. In the SW-RBS connection, the arcs were chords cut from a tube of 279.3 mm diameter. The perpendicular length between the two edges of the semi-circular parts ( $S$ ) (see Figure 1(b)) was about 20 cm, which was larger than the diameter of the tube in the HTW-RBS connection (about 11.4 cm). In this way, the length of the plastic area was increased, along with increases in stability, energy dissipation and ductility. The existence of an arc region in the web of a beam increases the out-of-plane stiffness of an AW. To increase the nominal plastic resistance at the column face and to reduce the ratio of maximum requirement moment to nominal plastic resistance is approximately 0.9. The accordion part of the web in the HTW-RBS connection was made by a tube of diameter 114 mm and thickness about 6 mm. The lengths of the column and beam were 2000 mm and 1850 mm, respectively. The beam and column sections were both seismic compression.

Figure 2 shows details of the SW-RBS connection and the AW parts. The beam flanges were connected to the column with pre-approved complete penetration slot welds (CPSWs) without any stiffener with a root pass and strengthening haunch. The continuity plates of the column were connected to the flanges of the column with CPSWs. The tubes and web of the beam between the columns and the beginning of the tube were connected to the beam flange with CPSWs. The web of the column was welded to the flanges in the panel zone, at distances of 30 cm higher and 30 cm lower than the beam, with CPSWs. The other joints, including the web of the beam to the column and the tubes to the web of the beam were welded with fillet welds. All the slot welds were ultrasonically tested by a specialist inspector.

For the beams, columns, continuity plates and tubes, A36 steel with a nominal yield stress of 240 MPa was used. The mechanical properties of steel coupons were tested according to ASTM A370 and the results are shown in Table 1.

### 3.2 Equipment and test setup

The test setup comprised a roller support at the base of the columns and two external frames placed at the location of applied load to maintain experimental boundary conditions. The columns had lateral supports to prevent out-of-plane movement of the specimen, lateral torsional buckling and local instability at the loading point. The boundary conditions of the beams consisted of roller supports at the free ends of the beams to prevent vertical movement. The distance of the frame (to prevent sideways movement of the beam) to the column centre was 85 cm. Displacement loading was applied to the top of the column by means of a hydraulic jack with a load capacity of 500 kN and displacement capacity of 250 mm. The test setup and overall dimensions of the SW-RBS connection are shown in Figure 3. The specimens were subjected to quasi-static loading according to AISC 341-10 (AISC, 2010). The total storey drift was calculated by dividing the

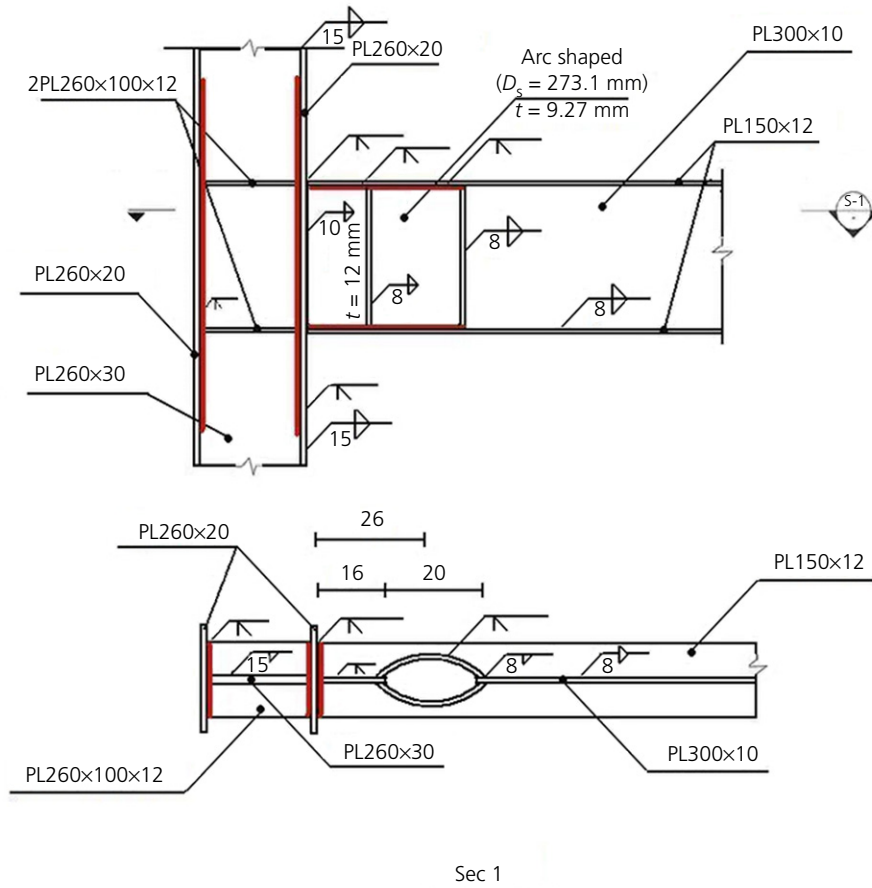


Figure 2. SW-RBS test specimen connection details (dimensions in mm). PL, plate

Table 1. Mechanical properties of steel coupons taken from different components of test subassembly

Member	Coupon	Yield strength: MPa	Tensile strength: MPa	Elongation: %
Beam	Web	288	446	40.5
Beam	Flange	268	384	40
Column	Web	260	419	45.5
Column	Flange	253	424	45
Pipe	—	295	447	38

displacement by the column height. Following AISC 341-10 (AISC, 2010), the load cycles applied to the specimens were six cycles of 0.375%, 0.5% and 0.75% storey drifts, four cycles of 1% drift and two cycles each of 1.5% and higher drifts. The rotations of the plastic hinges of the SW-RBS and HTW-RBS connections were measured using six linear variable differential transformers (LVDTs). The behaviour of the panel zone was assessed by means of two LVDTs arranged diagonally. As shown in Figure 4, strain gauges were placed at different points in the connection, including on the beam flange, beam web and tube to measure the strain history. Two external LVDTs were used to measure the horizontal displacement of the jack at top

of the column. The applied load was measured by a load cell placed behind the jack. The data sent by the strain gauges and the LVDTs were recorded by a digital data logger.

#### 4. Experimental results

To compare the SW-RBS and HTW-RBS connections, the cyclic behaviour of the specimens was investigated by testing and analysing the obtained information. For complete understanding of the behaviour of the specimens, the test results were compared with the results of a TW-RBS connection (Saleh *et al.*, 2016b).



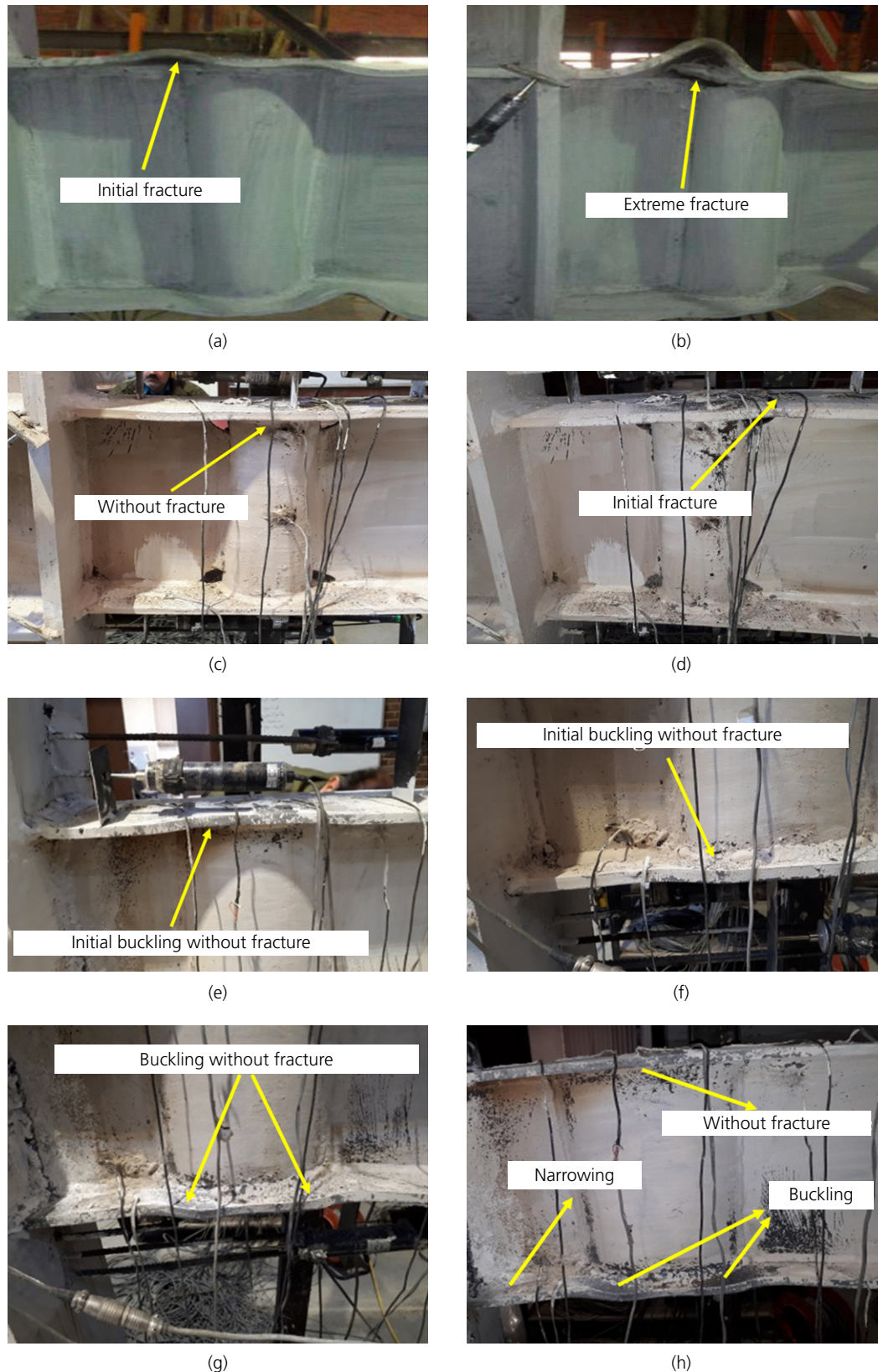


**Figure 5.** Test specimens and plastic hinges under cyclic loading: (a) TW-RBS specimen (Saleh *et al.*, 2016b), 5% storey drift; (b) TW-RBS specimen, 6% storey drift; (c) HTW-RBS specimen, 5% storey drift; (d) HTW-RBS specimen, 6% storey drift; (e) SW-RBS specimen, 5% storey drift; (f) SW-RBS specimen, 6% storey drift; (g) SW-RBS specimen, 7% storey drift; (h) SW-RBS specimen, 8% storey drift

beginning of 8% drift storey and at a force greater than the 7% storey drift force (about 18 750 kg), necking in the bottom flange occurred and the steel was torn (Figure 5(h)).

Loading in the SW-RBS connection was continued to the reverse cycle of 8% drift and the flexural strength of connection increased. It was not possible to continue cyclic loading due to fracture in the lower part of flange. However, with continuing the inverse cycle in the form of monotonic loading, the flexural strength of the connection increased. Loading was continued monotonically until 10% storey drift and no fracture in the upper flange of the beam occurred. Due to expansion of the weld failure at the beam–column connection and dropping of the flexural strength of the specimen, loading was stopped at 11% storey drift.

#### 4.2 Comparison of behaviour of specimens

For comparison of the SW-RBS and HTW-RBS connections, the hysteresis curves (load at top of the column against total storey drift) of both specimens are shown in Figure 6. The total storey drift was calculated by dividing the column tip displacement by the distance from the column base to the centreline (CL) of the actuator. Both specimens revealed quite stable inelastic behaviours and favourable energy dissipation capacities. The proposed connections satisfied the seismic acceptance criterion of AISC 341-10 (AISC, 2010) that the flexural capacity of the specimen at the column face should not be less than 80% of the beam plastic moment at 0.04 rad. As shown in Figure 6, until 7% storey drift, the strength degradation of both specimens remained less than 20%. The superiority of SW-RBS compared with HTW-RBS is due to expansion of the plastic hinge to the entire arc length (reduced area), which resulted in negligible buckling in the other parts and sinking only in the reduced area and in the arc regions. Therefore, the flexural capacity was increased. The decreasing

stress concentration in SW-RBS compared with HTW-RBS is due to increase of the length of the plastic hinge. Moreover, the existence of the arc shape in the SW-RBS connection rather than tube in the HTW-RBS connection resulted in better behaviour in terms of the stress in the connection. In the SW-RBS connection, by eliminating stress concentration points, the specimen was able to experience a higher storey drift, fatigue due to the stress concentration was reduced, and fractures and cracks at the connection of flanges and web to the steel tube were prevented.

For better understanding of the behaviour of the SW-RBS connection under the applied load, Figure 7 shows the beam moment at the column face plotted against the storey drift. The rotation was calculated by dividing the difference between LVDT 9 and LVDT 10 by their vertical spacing. This rotation relates to the plastic rotation of the beam, including the elastic rotation on the column face and also before the plastic area.

Figure 9 shows the normalised strain of the upper flange of the beam in SW-RBS, HTW-RBS and TW-RBS connections at 4% storey drift in the longitudinal direction. In all specimens, the strain was concentrated at the centre of the reduced area (arch shapes of the curves). The decreased strain of the reduced area in the SW-RBS connection compared with the TW-RBS connection shows how well the proposed AW behaved in the SW-RBS connection.

The strains at the middle of the arch and tube web were quite small; this shows the elimination of the contribution of this part to the flexural capacity of the connection. In all three specimens, the amount of strain in the reduced area compared with the column face was about three times larger. This indicates that the demand of plastic strain in the column face was reduced and the possibility of failure in the reduced region was greater than that in the area near the beam–column connection.

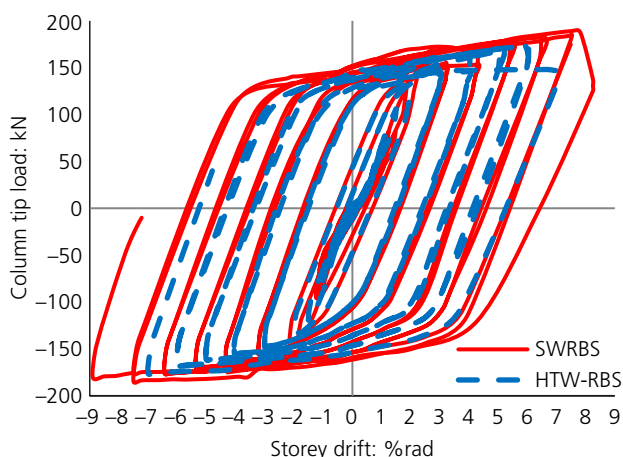


Figure 6. Comparison of cyclic responses of SW-RBS and HTW-RBS connections

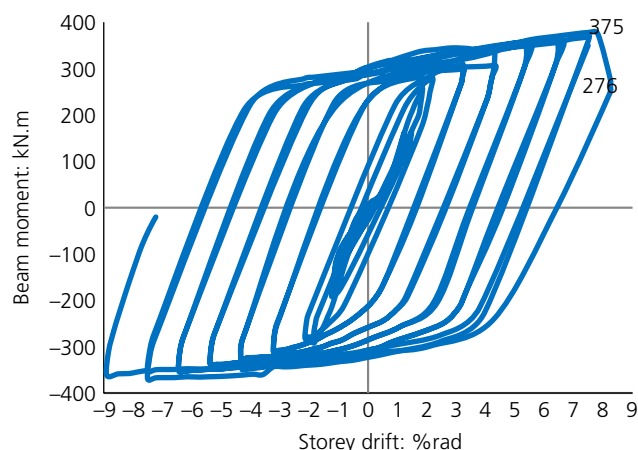


Figure 7. SW-RBS connection: beam moment at column face plotted against storey drift

## 5. Verification and comparison of results

The results in Figure 6 show that the ductility of the SW-RBS connection was greater than that of the HTW-RBS connection (it had a larger curve and lasted up to 7% storey drift without dropping the bending more than 20%). This can be attributed to the increased length of the plastic hinge and, consequently, increased non-linear rotation of the beam.

To understand the behaviour of the flange in the reduced area and to compare it with points close and far from the column face, the normalised strain curves ( $\epsilon/\epsilon_y$ ) at 26 cm (centre of the reduced area) and at 4% storey drift are shown in Figure 8. As shown in the figure, according to the increase of plastic area, local buckling at 26 cm from the column face (centre of reduced section) in the SW-RBS connection was decreased (compared with the HTW-RBS and TW-RBS connections). The strain in the SW-RBS connection was about 30% less than the strain in the TW-RBS connection and about 15% less than that in the HTW-RBS connection. According to the curves in Figure 8, because of the increase in the plastic hinge length in the SW-RBS connection, the length of the increased strain area was greater than that of the HTW-RBS and TW-RBS specimens; that is, the plastic hinge occurs over a greater length.

Figure 9 shows the normalised strain of the specimens at the width of beam top flange. It can be seen that the plastic hinge was formed in the middle of the width of beam top flange. The SW-RBS connection showed the most suitable behaviour, with the plastic hinge located far from the column face.

Figure 10(a) shows the normalised strain of the TW-RBS connection at the centre of the tube (plastic hinge area). The normalised strain of the HTW-RBS connection at the centre of the plastic hinge area is shown in Figure 10(b).

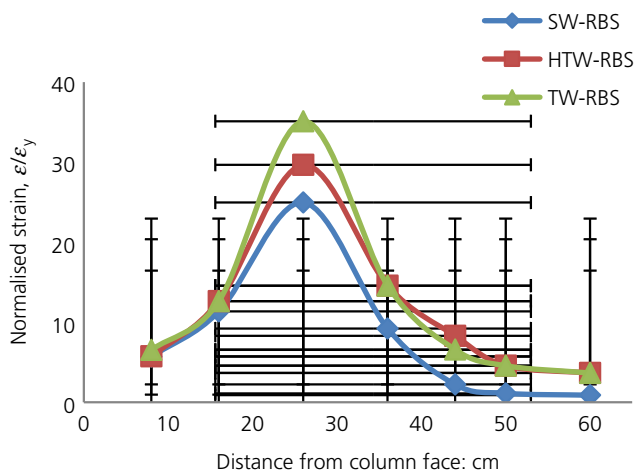


Figure 8. Comparison of normalised longitudinal strain profile along the beam top flange

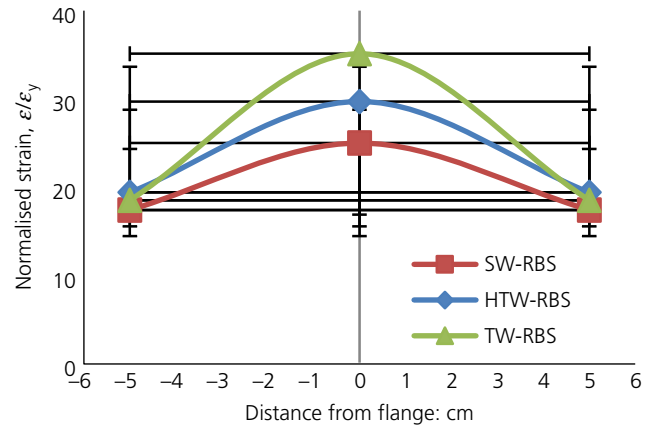


Figure 9. Comparison of normalised strain profile at the width of beam top flange

For the SW-RBS connection, the normalised strain at the centre of plastic hinge (26 cm from column face) is shown in Figure 10(c). All the curves are plotted together in Figure 10(d) for comparison. The figure shows that the strain in SW-RBS was less than in other specimens, due to the increase in the length of the plastic hinge area. The behaviour of the SW-RBS connection under LCF was improved and fatigue due to stress concentration was reduced due to use of the semi-circular shapes instead of the tube. The behaviour of the SW-RBS connection was better than the other specimens in terms of the distribution of strain.

## 6. Comparison of fatigue

### 6.1 LCF life

Dusicka *et al.* (2007) studied the effective length of the reduced section. The specimen dimensions are shown in Figure 11. Dusicka *et al.* (2007) assessed LCF based on the strain amplitudes and conducted a test programme to calculate the fatigue life. As shown in Figure 12, when the amount of strain decreased, the fatigue life of all specimens increased.

Fatigue life in a connection under low-cycle loading with a large plastic strain range is calculated by the Manson–Coffin rule (Coffin, 1954; Manson, 1954), given by

$$1. \quad \frac{\Delta\epsilon}{2} = \frac{\sigma_f'}{E} (2N_f)^b + \epsilon_f' (2N_f)^c$$

in which  $\Delta\epsilon$  is the strain range and  $N_f$  is the number of cycles to specimen failure.  $\sigma_f'$  and  $b$  are the fatigue strength coefficient and exponent, respectively, and  $\epsilon_f'$  and  $c$  are the fatigue ductility coefficient and exponent, respectively.  $E$  is the elastic modulus. These values for various steels are presented in Table 2. The values of the constants in Equation 1 used in this work were obtained from LYP-225 steel.

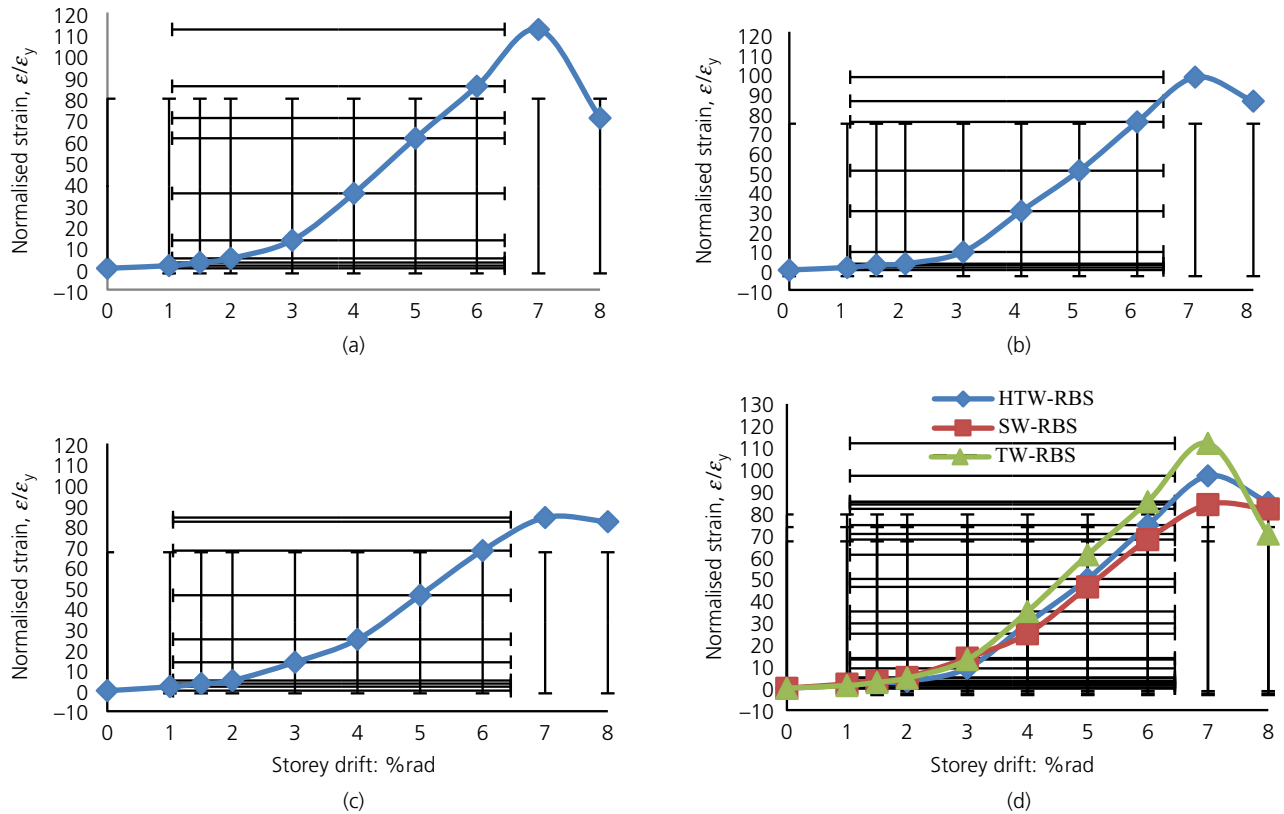


**Figure 10.** Normalised strain against storey drift: (a) TW-RBS specimen; (b) HTW-RBS specimen; (c) SW-RBS specimen; (d) comparison of specimens

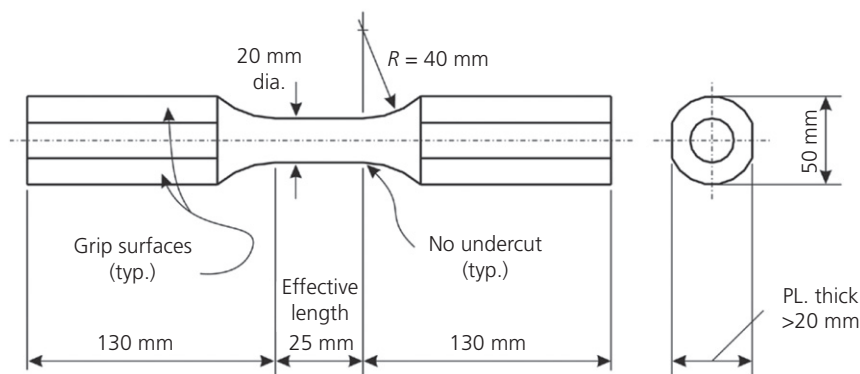


**Figure 11.** Dimensions of specimen studied by Dusicka *et al.* (2007). PL, plate

The cumulative fatigue damage of the SW-RBS, HTW-RBS and TW-RBS connections was calculated by substituting the values of  $\sigma_f$ ,  $E$ ,  $b$ ,  $c$  and  $\epsilon_f$  in Equation 1. As shown in Table 3, the cumulative fatigue damage ( $D$ ) in the SW-RBS was decreased by more than 35% in comparison with the TW-RBS connection; this is due to the decrease in stress concentration in SW-RBS. Compared with the HTW-RBS connection, the cumulative fatigue damage in the SW-RBS was reduced by

approximately 20%. The existence of the arc shape in the web of the SW-RBS connection decrease fatigue caused by a stress concentration near the plastic hinge. In the HTW-RBS connection, the fatigue caused by stress concentration at the connection of the tube and beam was also decreased and no fractures or cracks occurred at this area. The holes created on the beam web as a second fuse were actuated after the tube (primary fuse) and the length of the plastic hinge was increased.

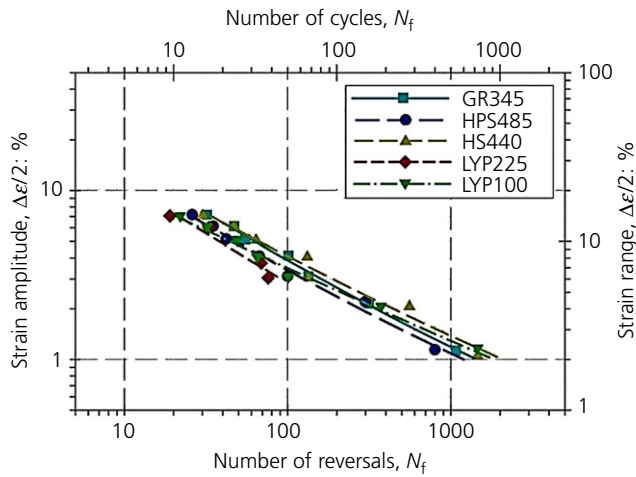


Figure 12. LCF life of five steels

Table 2. Coffin–Manson fatigue life coefficients

	LYP225	LYP100	HT400	HPS485	GR345
$\sigma_f$	507	475	1000	886	894
$b$	-0.063	-0.081	-0.101	-0.072	-0.082
$c_f$	0.446	0.275	0.422	0.432	0.535
$c$	-0.612	-0.459	-0.524	-0.0575	-0.590

## 6.2 Cumulative fatigue damage

(Vayas *et al.*, 2003) presented key results to calculate the  $\Delta\phi$ – $N_f$  fatigue deformability curve defined by

$$2. \quad \Delta\phi^m N_f = K$$

where  $\Delta\phi$  is the total rotation range,  $N_f$  is the number of cycles to failure,  $m$  is the slope of the fatigue curve and  $K$  is a constant. The parameters  $m$  and  $K$  for each connection were obtained from test data.

To assess the cumulative fatigue damage, the Palmgren–Miner' rule (Miner, 1945; Palmgren *et al.*, 1924) was used. The

Palmgren–Miner equation is

$$3. \quad D = \sum_{i=1}^k \frac{n_i}{N_{f_i}} = \sum_{i=1}^k \frac{n_i \Delta\phi_i^m}{K}$$

where  $n_i$  is the number of cycles to reach rotation range  $\Delta\phi_i$ ,  $N_{f_i}$  is the number of cycles to failure at rotation range  $\Delta\phi_i$ ,  $k$  is the number of blocks with different rotation ranges and  $D$  is the cumulative fatigue damage (ranging between 0 (no damage) and 1 (complete damage)).

To calculate  $m$  and  $K$  in Equation 3, tests need to be conducted and the results are obtained from fatigue deformability curves. For this study, the US-RBS connection was chosen for obtaining  $m$  and  $K$ . The US-RBS category is very similar to the proposed connection. The values of  $m$  and  $K$  for the US-RBS were determined to be 3 and  $1.93 \times 10^{-3}$ , respectively.

After substituting the values of  $m$  and  $K$  in Equation 3, the cumulative fatigue damage ( $D$ ) was calculated, as shown in Table 4. The value of  $D$  was between 0 and 1. Until 7% storey drift, the cumulative fatigue damage was thus in a suitable range.

## 7. Numerical study

To compare the experimental and numerical results, the SW-RBS, HTW-RBS and TW-RBS (Saleh *et al.*, 2016b) connections were simulated by FE modelling.

### 7.1 Modelling and FE analysis

Abaqus (HKSI, 1997) was used to create three-dimensional models of the connections. The geometry of the beams, columns and curved parts was exactly the same as used in the experiments.

Flexible shell elements were used to model the beams, columns and curved parts. A four-node element with six degrees of freedom was used for meshing. To achieve the desired number of elements, the strain parameter was considered. In the next step, the number of elements was doubled (the dimensions of

Table 3. Cumulative fatigue damage according to the Coffin–Manson rule

Storey drift	TW-RBS		HTW-RBS		SW-RBS	
	$\Delta\epsilon$	$N_f$	$\Delta\epsilon$	$N_f$	$\Delta\epsilon$	$N_f$
1.5%	0.00531	7140	0.0051	8218	0.00676	3640
2%	0.00926	780	0.0063	4415	0.00992	1420
3%	0.0262	118	0.0182	402	0.02760	183
4%	0.0702	44	0.0594	47	0.05010	61
5%	0.1220	14	0.1010	19	0.06260	41
6%	0.1701	8	0.1490	10	0.14701	10
7%	0.2241	5	0.1942	6	0.18840	7
$D = \sum n_i/N_{f_i}$	0.85		0.69		0.58	

**Table 4.** Cumulative fatigue damage according to the Palmgren–Miner rule for HTW-RBS

$\Delta\phi_i$	$n_i$	$n_i\Delta\phi_i^3/(1.93 \times 10^{-3})$
0.00375	6	0.0001639
0.005	6	0.0003886
0.0075	6	0.0013115
0.01	4	0.0020725
0.015	2	0.0034974
0.02	2	0.0082902
0.03	2	0.0279793
0.04	2	0.0663212
0.05	2	0.1295337
0.06	2	0.2238342
0.07	2	0.3554404
$D = \sum n_i\Delta\phi_i^3/(1.93 \times 10^{-3})$		0.818833

each element were halved) and the solution was repeated to measure the effect of mesh thinning. The process was continued until a balance was struck between time and the number of elements. In other words, as the number of elements was increased, there was no significant change in the solution. In fact, the cost of calculations overcame the changes in the answers: when the answers converged there was no need to use more elements as increasing the number of elements does not help increase the accuracy of the solution but only increases the solution time. The minimum element size that was found to produce satisfactory results was 17.5 mm. The mesh size of the column was 25 mm and the mesh size of the beam flange and web was considered as 17.5 mm due to sensitivity in analysis.

The model of the SW-RBS connection consisted of 7955 nodes and 7494 linear quadrilateral elements of type S4R. The HTW-RBS connection model consisted of 7933 nodes and 7474 linear quadrilateral elements of type S4R. The TW-RBS connection consists of 7810 nodes and 7356 linear quadrilateral elements of type S4R.

A tie constraint was used to restrain the degrees of freedom. For applying detail of the experiments, kinematic hardening was used for the plastic properties of the members. The yield stress and tensile strength of the material shown in Table 1 were used to model the components. In the analysis, Young's modulus of elasticity and Poisson's ratio of all materials were taken as 203 GPa and 0.3, respectively. For acceptable numerical analysis, the boundary conditions and their locations were applied exactly as in the experimental specimens. According to AISC 341-10 (AISC, 2010), the specimens were loaded at the top of the column with displacement occurring there.

## 7.2 Numerical results

The numerical and experimental results of the SW-RBS connection are shown in Figure 13. The experimental and numerical curves of applied load at top of the column against storey drift show good agreement.

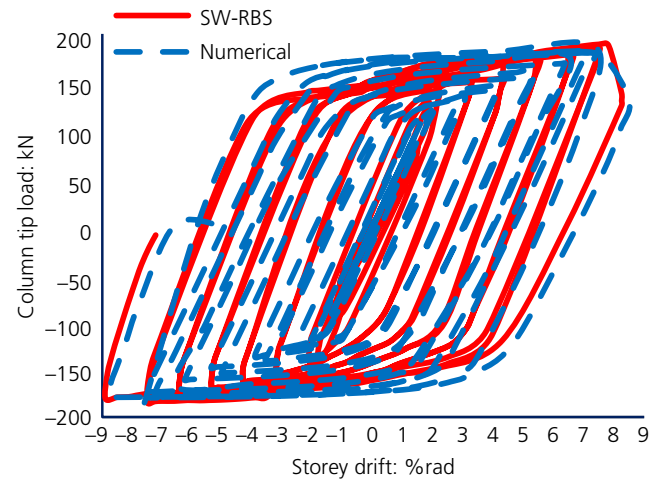
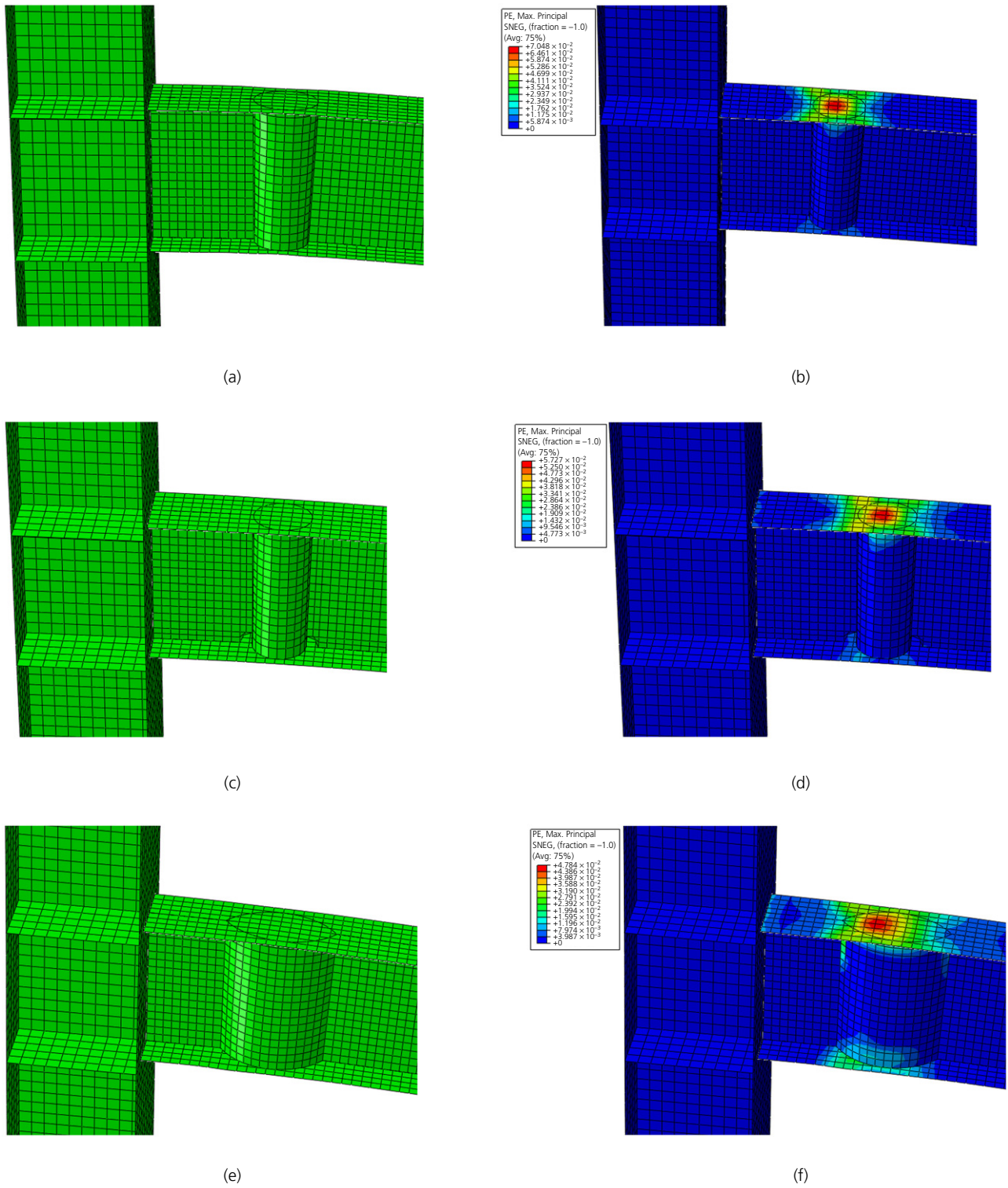
**Figure 13.** Comparison of numerical and experimental results of SW-RBS connection

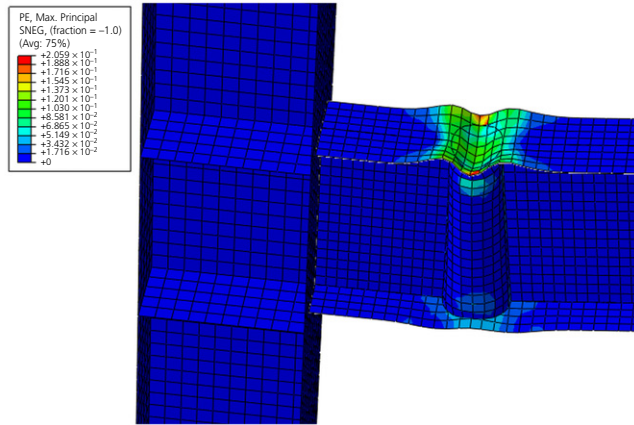
Figure 14 shows the locations of the plastic hinge in SW-RBS, HTW-RBS and TW-RBS (Saleh *et al.*, 2016b) at 4% storey drift. Figures 14(a), 14(c) and 14(e) show the deformed shapes of the SW-RBS, HTW-RBS and TW-RBS connections, respectively. Opening and stretching of the tube and curved parts in the beam web show the good behaviour of the AWs. Figures 14(b), 14(d) and 14(f) show the von Mises plastic strain distributions in the SW-RBS, HTW-RBS and TW-RBS connections. The increase in the plastic hinge length decreased the stress concentration in the SW-RBS connection and the LCF in the beam was reduced. Compared with the HTW-RBS and TW-RBS connection, the strain level was decreased in the SW-RBS connection, thus improving the behaviour of the structure.

As shown in Figure 15, the final results of the experiment at 7% storey drift showed good agreement with the numerical results and prediction of the locations of buckling and the plastic hinge. Figures 15(a) and 15(b) show the numerical and experimental results of the TW-RBS connection (Saleh *et al.*, 2016b). As shown in Figure 15(b), after extreme buckling in the top flange, the beam flange separated from the tube and fracture occurred. Figures 15(c) and 15(d) shows the results for the HTW-RBS connection. The prediction of the behaviour of specimen was good and location of the plastic hinge was predicted well. As shown in Figure 15(d), there was no fracture in the connection of the beam flange to the tube. Increasing the length of the plastic hinge by adding a tube with holes in the beam web reduced the LCF and increased the seismic performance.

The numerical and experimental behaviour of the SW-RBS connection under cyclic loading is shown in Figures 15(e) and 15(f). Sinking at the bottom flange of the connection is evident in Figure 15(f), which indicates the acceptable



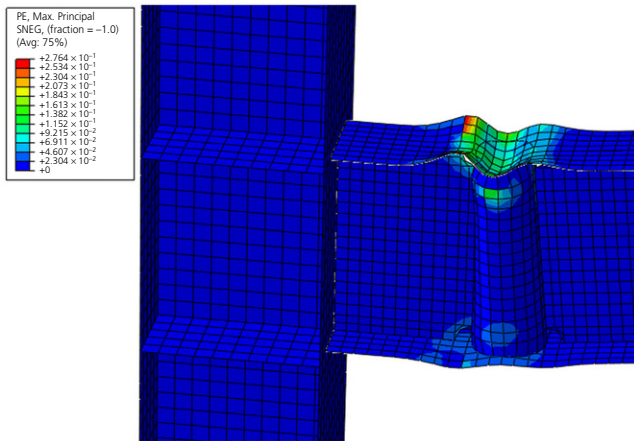
**Figure 14.** Numerical results of specimens at 4% storey drift: (a) deformed shape of TW-RBS connection; (b) von Mises plastic strain distribution in TW-RBS; (c) deformed shape of HW-RBS connection; (d) von Mises plastic strain distribution in HTW-RBS; (e) deformed shape of SW-RBS connection; (f) von Mises plastic strain distribution in SW-RBS



(a)



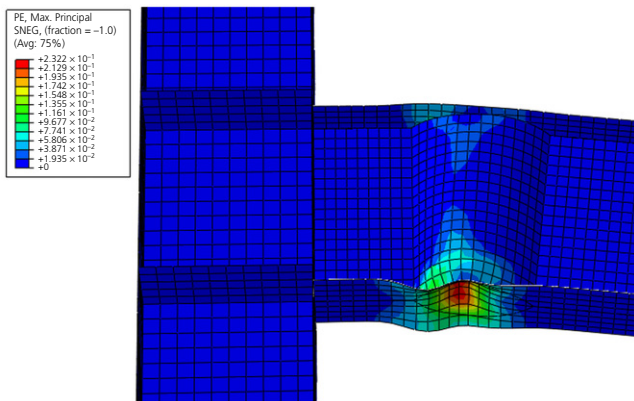
(b)



(c)



(d)



(e)



(f)

**Figure 15.** Comparison of final deformed experimental shapes and FE results: (a) von Mises plastic strain distribution in TW-RBS; (b) experimental result for TW-RBS; (c) von Mises plastic strain distribution in HTW-RBS; (d) experimental result for HTW-RBS; (e) von Mises plastic strain distribution in SW-RBS; (f) experimental result for SW-RBS

prediction of FE modelling. In summary, the numerical and experimental results of all the specimens showed good coincidence, which could help to predict the behaviour of other specimens. In addition to qualitative assessments, the fatigue parameter  $D$  was used to compare the predictions of joint failure. The lower the amount of fatigue damage, the less likely are flange detachment fractures at the junction of the flange.

## 8. Conclusions

In this work, LCF due to stress concentrations in different types of RBS connections was compared. A new type of RBS connection, called the SW-RBS, is proposed. In this connection, the flat web of the beam is replaced by two semi-circular parts; this moves the plastic hinge to the desired location (the same place as the arcs of the semi-circular parts), away from the column face. An experimental and numerical study was conducted to investigate the connection and the results were compared with the results of previous research studies including the HTW-RBS of Nadi *et al.* (2020) and the TW-RBS of Saleh *et al.* (2016b). The following conclusions were drawn from this work.

- Compared with the other connections, the SW-RBS connection showed more ductility at 7% storey drift without more than 20% loss of strength so, according to Fema (2000) and AISC (2010), it can be categorised as a rigid connection. The proposed connection also tolerated 10% storey drift under monotonic loading and showed better performance than the HTW-RBS connection under seismic loading.
- Because the AW in the SW-RBS connection is made from semi-circles, LCF was reduced significantly in comparison with the HTW-RBS and TW-RBS connections.
- The SW-RBS connection can be constructed easily and quickly: placing arcs on a flat web is not as difficult as placing a pipe or an angle in the web of a beam.
- Due to the decrease in stress concentration, the strain in the SW-RBS connection was about 30% less than the strain of the TW-RBS connection and about 15% less than the strain of the HTW-RBS connection.
- Compared with the TW-RBS connection, the cumulative fatigue damage in the SW-RBS connection was decreased by more than 35% due to the decrease in stress concentration at connection. In comparison with the HTW-RBS connection, the cumulative fatigue damage in the SW-RBS connection was reduced by approximately 20%.
- The demand of the beam–column connection decreased by more than 35% compared with other points; this indicates better seismic behaviour than single- and double-pipe TW-RBS connections.
- Comparison of the numerical and experimental results showed the acceptable predictions of the FE models, which could help to predict the behaviour of other specimens.

- Due to the decrease in LCF in the SW-RBS connection, there was no separation between the flange of the beam and the AW.

## Acknowledgement

The authors thank the Building and Housing Research Center of Iran for conducting the tests, especially Dr Farhang Farahbod for his valuable advice during the experimental tests. The authors declare that they have no known competing financial interests or personal relationships that could have appeared to influence the work reported in this paper.

## REFERENCES

- AISC (American Institute of Steel Construction) (2010) ANSI/AISC 341-10: Seismic provisions for structural steel buildings. AISC, Chicago, IL, USA.
- Amiri A and Anderson JC (2012) Effect of low cycle fatigue on steel moment frame with RBS. In *Behaviour of Steel Structures in Seismic Areas* (Mazoolani F and Herrera R (eds)). CRC Press, Boca Raton, FL, USA.
- ASTM (2019) A370-19: Standard test methods and definitions for mechanical testing of steel products. ASTM International, West Conshohocken, PA, USA.
- Barsom JM (2002) Development of fracture toughness requirements for weld metals in seismic applications. *SAC Steel Project Task 7(1)*: 3.
- Bhatti NA, Pereira K and Wahab MA (2019) Effect of stress gradient and quadrant averaging on fretting fatigue crack initiation angle and life. *International Journal of Tribology* **131**: 212–221.
- BSI (2004) BS EN 1998-1:2004: Eurocode 8. Design of structures for earthquake resistance. General rules, seismic actions and rules for buildings. BSI, London, UK.
- Coffin Jr LF (1954) A study of the effects of cyclic thermal stresses on a ductile metal. *Transgenderism* **76(6)**: 931–950.
- Deng Q, Bhatti NA, Yin X and Wahab MA (2018) Numerical modeling of the effect of randomly distributed inclusions on fretting fatigue-induced stress in metals. *Journal of Metals* **8(10)**: 836–856.
- Deng Q, Bhatti NA, Yin X and Wahab MA (2020) The effect of a critical micro-void defect on fretting fatigue crack initiation in heterogeneous material using a multiscale approach. *International Journal of Tribology* **141**: 105909.
- Dusicka P, Itani AM and Buckle IG (2007) Cyclic response of plate steels under large inelastic strains. *Journal of Constructional Steel Research* **63(2)**: 156–164.
- Fema (Federal Emergency Management Agency) (2000) *State of The Art Report on Connection Performance*. Fema, Washington, DC, USA, Fema-355D.
- HKSI (Hibbit, Karlsson and Sorensen, Inc.) (1997) *Abaqus User Manual*. HKSI, Providence, RI, USA.
- Huang YL and Mahin SA (2010) *Simulating the Inelastic Seismic Behavior of Steel Braced Frames Including the Effects of Low-Cycle Fatigue*. Pacific Earthquake Engineering Research Center, University of California, Berkeley, CA, USA, PEER report 2010/104.
- Imanpour A, Torabian S and Mirghaderi SR (2019) Seismic design of the double-cell accordion-web reduced beam section connection. *Engineering Structures* **191(1)**: 23–38.
- Jones SL, Fry GT and Engelhardt MD (2002) Experimental evaluation of cyclically loaded reduced beam section moment connections. *Engineering Structures* **128(4)**: 441–451.
- Kosec G, Slak J, Depolli M, Trobec R and Wahab MA (2019) Weak and strong from meshless methods for linear elastic problem under

- fretting contact conditions. *International Journal of Tribology* **138**: 392–402.
- Kuwamura H (1998) Fracture of steel during an earthquake – state-of-the-art in Japan. *Engineering Structures* **20(4–6)**: 310–322.
- Lashkari B (1988) Seismic risk evaluation of steel structures based on low-cycle fatigue. *Reliability Engineering & System Safety* **20(4)**: 297–302.
- Lee K and Stojadinovic B (2004) Low-cycle fatigue limit on seismic rotation capacity for US steel moment connections. *Proceedings of International 13th World Conference on Earthquake Engineering, Vancouver, BC, Canada*, Paper No. 90.
- Malley JO (1998) SAC steel project: Summary of phase I testing investigation results. *Engineering Structures* **20(4–6)**: 300–309.
- Manson SS (1954) *Behavior of Materials Under Conditions of Thermal Stress*. National Advisory Commission for Aeronautics, Washington, DC, USA, No. 1170.
- Miner MA (1945) Cumulative damage in fatigue. *Journal of Applied Mechanics, Transactions ASME* **12(3)**: 159–164.
- Mirghaderi SR, Torabian S and Imanpour A (2010) Seismic performance of the accordion web RBS connection. *Journal of Constructional Steel Research* **66(2)**: 277–288.
- Nadi A, Saleh A and Ayazi A (2020) Fatigue reduction in tubular web connections in semi-deep beam. *International Journal of Steel Structures* **20(4)**: 1193–1208.
- Nastar N, Anderson JC, Brandow GE and Nigbor RL (2010) Effects of low-cycle fatigue on a 10-storey steel building. *Structural Design of Tall and Special Buildings* **19(1–2)**: 95–113.
- Nastar N, Brandow G, Anderson J and Nigbor RL (2012) The effects of low-cycle fatigue in steel structures. *Forensic Engineering* **10(3)**: 1121–1130.
- Palmgren AG, Lebensdauer D and Kugellagern V (1924) Life length of roller bearings. *Zeitschrift des Vereines Deutscher Ingenieure* **68(14)**: 339–341.
- Papagianni D and Wahab MA (2020) Multi-scale analysis of fretting fatigue in heterogeneous materials using computational homogenization. *Computers, Materials and Continua* **62(1)**: 79–97.
- Pereira K and Wahab MA (2020) Fretting fatigue lifetime estimation using a cyclic cohesive zone model. *International Journal of Tribology* **141**: 105899.
- Ricles JM, Mao C, Lu LW and Fisher JW (2000) *Development and Evaluation of Improved Details for Ductile Welded Unreinforced Flange Connections. Final Report. SAC Task 7.05*, Washington, DC, USA, ATLSS Report No. 00-04.
- Ricles JM, Mao C, Lu LW, Fisher JW et al. (2002) Inelastic cyclic testing of welded unreinforced moment connections. *Journal of Structural Engineering* **128(4)**: 429–440.
- Saleh A, Zahrai SM and Mirghaderi SR (2016a) Experimental study on innovative tubular web RBS connections in steel MRFs with typical shallow beams. *Structural Engineering & Mechanics* **57(5)**: 785–808.
- Saleh A, Mirghaderi SR and Zahrai SM (2016b) Cyclic testing of tubular web RBS connections in deep beams. *Journal of Constructional Steel Research* **117**: 214–226.
- Tateishi K and Hanji T (2004) Low cycle fatigue strength of butt-welded steel joint by means of new testing system with image technique. *International Journal of Fatigue* **26(12)**: 1349–1356.
- Uang CM and Chi B (2002) Cyclic response and design recommendations of RBS moment connections with deep column. *Journal of Structural Engineering* **128(4)**: 464–473.
- Vayas I, Sophocleous A and Dinu F (2003) Fatigue analysis of moment resisting steel frames. *Journal of Earthquake Engineering* **7(4)**: 635–654.
- Wang X, Zhang W, Gong J and Wahab MA (2018) Low cycle fatigue and creep fatigue interaction behavior of 9Cr-0.5Mo-1.8W-V-Nb heat-resistant steel at high temperature. *Journal of Nuclear Materials* **505**: 73–84.
- Wang X, Zhang W, Zhang T, Gong J and Wahab MA (2019) A new empirical life prediction model for 9–12%Cr steels under low cycle fatigue and creep fatigue interaction loadings. *Metals* **9(2)**: 183.
- Zahrai SM, Mirghaderi SR and Saleh A (2017a) Tubular web reduced beam section (TW-RBS) connection, a numerical and experimental study and result comparison. *Steel and Composite Structures* **23(5)**: 421–433.
- Zahrai SM, Mirghaderi SR and Saleh A (2017b) Increasing plastic hinge length using two pipes in a proposed web reduced beam section, an experimental and numerical study. *Steel and Composite Structures* **23(4)**: 421–433.
- Zhang W, Wang X, Ni J et al. (2018) Influence of prior low cycle fatigue on microstructure evolution and subsequent creep behavior. *International Journal of Fatigue* **109**: 114–125.
- Zhang X and Ricles JM (2006) Experimental evaluation of reduced beam section connections to deep columns. *Journal of Structural Engineering* **132(3)**: 346–357.
- Zhou H, Wang Y, Yang L and Shi Y (2014) Seismic low-cycle fatigue evaluation of welded beam-to-column connections in steel moment frames through global-local analysis. *International Journal of Fatigue* **64**: 97–113.

